

Article

Speed-Adaptive Model-Free Path-Tracking Control for Autonomous Vehicles: Analysis and Design

Marcos Moreno-Gonzalez ^{1,*}, Antonio Artuñedo ¹ , Jorge Villagra ¹ , Cédric Join ^{2,3} and Michel Fliess ^{2,4}

¹ Centre for Automation and Robotics (CAR), CSIC—Universidad Politécnica de Madrid, Ctra. M300 Campo Real, km 0, 200, Arganda del Rey, 28500 Madrid, Spain; antonio.artunedo@csic.es (A.A.); jorge.villagra@csic.es (J.V.)

² AL.I.E.N., 7 rue Maurice Barrès, 54330 Vézelize, France; cedric.join@alien-sas.com (C.J.); michel.fliess@alien-sas.com (M.F.)

³ CRAN (CNRS, UMR 7039), Université de Lorraine, BP 239, 54506 Vandoeuvre-lès-Nancy, France

⁴ LIX (CNRS, UMR 7161), École Polytechnique, 91128 Palaiseau, France

* Correspondence: marcos.moreno@csic.es

Abstract: One of the challenges of autonomous driving is to increase the number of situations in which an intelligent vehicle can continue to operate without human intervention. This requires path-tracking control to keep the vehicle stable while following the road, regardless of the shape of the road or the longitudinal speed at which it is moving. In this work, a control strategy framed in the Model-Free Control paradigm is presented to control the lateral vehicle dynamics in a decoupled control architecture. This strategy is designed to guide the vehicle through trajectories with diverse dynamic constraints and over a wide speed range. A design method for this control strategy is proposed, and metrics for trajectory tracking quality, system stability, and passenger comfort are applied to evaluate the controller's performance. Finally, simulation and real-world tests show that the developed strategy is able to track realistic trajectories with a high degree of accuracy, safety, and comfort.

Keywords: model-free control; autonomous vehicles; lateral control



Citation: Moreno-Gonzalez, M.; Artuñedo, A.; Villagra, J.; Join, C.; Fliess, M. Speed-Adaptive Model-Free Path-Tracking Control for Autonomous Vehicles: Analysis and Design. *Vehicles* **2023**, *5*, 698–717. <https://doi.org/10.3390/vehicles5020038>

Academic Editors: Zejiang Wang, Wenshuo Wang, Moad Kissai, Umar Zakir Abdul Hamid and Anh-Tu Nguyen

Received: 11 May 2023
Revised: 31 May 2023
Accepted: 6 June 2023
Published: 13 June 2023



Copyright: © 2023 by the authors. Licensee MDPI, Basel, Switzerland. This article is an open access article distributed under the terms and conditions of the Creative Commons Attribution (CC BY) license (<https://creativecommons.org/licenses/by/4.0/>).

1. Introduction

Over the last few years, a variety of driving assistance systems have become widespread. These functions make driving safer and more comfortable, but the presence of a human driver is still essential. To take the next step, a much higher level of autonomous capability is needed, allowing the vehicle to operate in a greater number of situations without the intervention of the driver. To this end, accurately controlling the vehicle in any driving situation is essential.

In a decoupled control architecture, which is commonly used in the literature, lateral control aims to guide the vehicle to stay on the path without losing stability or impairing passenger comfort, regardless of whether the road has sharp curves or the vehicle is traveling at high or low speeds. This problem has been addressed using different approaches, one of which involves improving the available model of the vehicle in order to better tune a model-based regulator, which is a very complex task due to the nonlinear and variant characteristics of the system. Some authors have attempted to design controllers for different speed-specific driving situations and provide a fitting law between the different parameters or outputs of the controllers. To avoid the problems induced by complex system identification, model-independent strategies are gaining interest.

Speed-Adaptive Model-Free Control (SAMFC) [1] is a path-tracking control strategy for autonomous vehicles framed within the Model-Free Control (MFC) paradigm [2]. It is based on the adaptation of one of the key parameters of MFC as a function of driving speed, allowing the vehicle to cope with a variety of situations without having to re-tune

the controller for any of them. In this paper, SAMFC is analyzed in a more formal and extensive way. To thoroughly evaluate the potential of this strategy in comparison with a standard MFC controller, metrics of tracking quality, stability of the feedback system, and passenger comfort are defined. A noniterative design procedure is proposed to obtain control configurations that meet specific time-response and frequency-response specifications. Therefore, the main contribution of this work lies in the introduction, analysis, and design procedure of an easy-to-implement variation of MFC, which has proven to be very effective for lateral control of automated vehicles.

The rest of this paper is structured as follows. Section 2 presents a brief review of lateral control strategies in the literature, focusing on model-independent approaches. A theoretical introduction to Model-Free Control is presented in Section 3. Section 4 introduces the proposed Speed-Adaptive Model-Free Control strategy and provides an analysis of its usefulness, as well as a design procedure. The results of the simulation and real-world tests are presented in Section 5. Finally, Section 6 presents some concluding remarks and references.

2. State-of-the-Art Literature

Lateral control of autonomous vehicles is studied from different approaches [3], most of which are based on a somewhat realistic model of the vehicle, with the single-track model being the most popular [4]. The success of this vehicle dynamics representation lies in its linear nature, which assumes a constant longitudinal velocity. Some real applications show that this simplification may be inappropriate for providing accurate lateral control in every driving circumstance. To overcome these limitations, different model-based feedback strategies have been proposed in the last few years. Ref. [5] applied the single-track model to fit two PID (Proportional-Integral-Derivative) regulators, one for low and one for high speeds. Ref. [6] used the model to synthesize a robust LQR (Linear Quadratic Regulator). Ref. [7] applied the Lyapunov theory to obtain an asymptotically stable regulator on an extended model. Another approach is gain scheduling, which was applied in [8] to control an electric vehicle. Alternatively, Model Predictive Control (MPC) strategies have also been developed and evaluated in real cars. Some of these strategies rely on a more complex model [9], whereas others focus on jointly solving the path-planning and control problems [10]. However, they are mainly tested in specific driving situations. In [11], a cascade MPC-PD structure was applied in a shared control architecture to perform an overtaking maneuver.

Real vehicles have complex dynamics that vary with speed and steering angle and have strong nonlinearities in the tire-ground interface, as well as the steering and suspension systems. Additionally, there are couplings between lateral and longitudinal dynamics, as well as variability in parameters that are already difficult to characterize such as wheel stiffness or inertia, which depends on the mass distribution within the vehicle. Consequently, it is extremely hard to find a realistic model that covers a wide range of driving situations. As a result, control strategies that do not rely on a vehicle dynamic model have attracted attention from the research community.

Fuzzy control is a good example of a model-free technique. It enables the control of nonlinear systems, absorbs some of the variability in the system parameters, and results in a formulation that is intuitive but difficult to tune optimally over a wide working range. Two fuzzy regulators were integrated and validated in traffic-based driving environments [12]. Other works [13,14] have confirmed the capabilities of fuzzy lateral control for autonomous vehicles. Another approach is pure pursuit control [15], which is based on a vehicle kinematic model. Although it behaves reasonably well at low speeds, its performance degrades when high velocities or accelerations are requested.

The MFC framework mentioned in the introduction has been successfully applied in vehicle longitudinal control applications [16] and in lateral control for low-speed Automated Guided Vehicles [17], as well as in other applications [18,19]. Alternatively, in [20], the flatness theory [21], which enables the identification of differentially flat outputs for

nonlinear systems, was applied to implement the lateral control of a vehicle together with a model-free feedback controller. This approach exhibited very good performance in simulation. However, its deployment in real vehicles is not straightforward, as it requires measurements that cannot be obtained using commercial sensors. A special case is Ultra-Local Model Predictive Control (ULMPC) [22], which is a unique combination of model-free and model-based approaches. This approach involves the application of an MPC regulator that uses a state representation of the ultra-local model proposed in MFC. However, the computational power required by ULMPC, although lower than that of MPC, is higher than that of MFC, as a real-time solver is still needed.

Alternatively, the authors of [23] proposed an adaptation mechanism for MFC and applied it on a scale car. However, the resulting adaptation dynamic is too slow for automated vehicles driving on real roads. Other examples of adaptation mechanisms for MFC can be found in the literature. The authors of [24] proposed an adaptation law for α based on the knowledge of the nominal model of the system. Similarly, the authors of [25] proposed an MFC-modified control structure and an adaptation law for α based on a Lyapunov function. Additionally, the authors of [26] proposed an adaptation law for α based on least squares estimation and applied it to a seven-degree-of-freedom upper-limb exoskeleton.

3. Model-Free Control Principles

Model-Free Control [2] is a newly developed control framework for SISO systems, which has demonstrated its performance across a wide variety of applications, as discussed in Section 2. This framework involves reducing the system's dynamics, which can be nonlinear, time-varying, or complex to identify, using a simple model that is updated online known as the ultra-local model (1).

A demonstration of this approximation is as follows. Assume that the dynamics of the considered SISO system can be defined by the algebraic differential equation $E(y, \dot{y}, \dots, y^{(a)}, u, \dot{u}, \dots, u^{(b)}) = 0$, which establishes a relationship between its input u and output y (along with their derivatives). Additionally, consider n as a non-negative integer such that $\frac{\partial E}{\partial y^{(n)}} \neq 0$, therefore $E(\cdot) = 0$ can be rewritten locally as $y^{(n)} = \varepsilon(y, \dot{y}, \dots, y^{(n-1)}, y^{(n+1)}, \dots, y^{(a)}, u, \dot{u}, \dots, u^{(b)})$. This equation yields the ultra-local model:

$$y^{(n)} = F + \alpha \cdot u \quad (1)$$

in which the relationship between the input u and the n th derivative of the output y of the system is considered linear, with a constant ratio α that is a design parameter. This linear relationship is fitted by a variable F that absorbs model errors and system disturbances.

Further, the feedback control is defined to reduce modeling and tracking errors, resulting in an *intelligent* controller:

$$u = \frac{1}{\alpha} \cdot \left(-F + y_r^{(n)} + \mathfrak{C}(e, \cdot) \right) \quad (2)$$

where u is the control action, $y_r^{(n)}$ is the n th derivative of the output reference, e is the tracking error, and $\mathfrak{C}(e, \cdot)$ is a classical controller expression.

Among the intelligent controllers, the iPD controller is the most widely used:

$$u = \frac{1}{\alpha} \cdot \left(-F + y_r^{(n)} + K_p e + K_d \dot{e} \right) \quad (3)$$

where K_p and K_d are the control parameters.

The term F has to be updated continuously and, therefore, must be estimated in real time using an estimator \hat{F} .

Implementation of Model-Free Controllers

The MFC controllers implemented in this paper are second-order iPDs ($n = 2$); therefore, (3) yields the control action u_{iPD} :

$$u_{iPD}(t_k) = \frac{-\hat{F}(t_k) + \dot{y}_{L,r}(t_k) + K_p e(t_k) + K_d \hat{e}(t_k)}{\alpha} \quad (4)$$

$$e(t_k) = y_{L,r}(t_k) - y_L(t_k); \quad \hat{e}(t_k) = \dot{y}_{L,r}(t_k) - \dot{y}_L(t_k)$$

where t_k is the current instant, y_L is the lateral deviation of the vehicle, e is the tracking error, and \hat{e} is the filtered estimation of the tracking error derivative.

In order to estimate F , various estimators can be considered, but in the remainder of this paper, a simple one is applied due to its high performance and low computational time. The estimator assumes that F remains constant between consecutive instants, allowing it to be estimated from previous control actions based on (1) as follows:

$$\hat{F}(t_k) = \hat{y}^{(n)}(t_k) - \alpha \cdot u(t_{k-1}) \quad (5)$$

where $\hat{y}^{(n)}$ is the estimation of the n th derivative of y . This estimation is obtained by applying the following filtered derivative operator n times to the output of the system:

$$D(z) = \frac{1}{T_s} \frac{1 - z^{-1}}{C + (1 - C) \cdot z^{-1}} \quad (6)$$

where T_s is the sample time and C is the filtering parameter, which is experimentally set at $C = 1.5$ so that the measurement noise is reduced.

4. Speed-Adaptive Model-Free Control

4.1. Introduction

Speed-Adaptive Model-Free Control (SAMFC) [1] is a variation of the original MFC structure that was specifically developed for the lateral control of autonomous vehicles. It was experimentally shown in [1] that the MFC control parameter α is inversely related to the aggressiveness of the controller. In lateral vehicle control, when the longitudinal speed of the vehicle is high, aggressive MFC controllers generate an oscillatory control action. In contrast, when the speed is low, smooth controllers do not accurately follow the curves of the path. Therefore, the variation of α (\sim aggressiveness) with longitudinal speed is justified.

Consequently, SAMFC proposes the following adaptation law:

$$\alpha(t_k) = \begin{cases} \alpha_0 & \text{if } v_x(t_k) < v_{x,0} \\ K_\alpha \cdot (v_x(t_k) - v_{x,0}) + \alpha_0 & \text{if } v_x(t_k) \geq v_{x,0} \end{cases} \quad (7)$$

where α is limited by α_0 , which is maintained up to a given speed $v_{x,0}$ and then proportionally increased to the longitudinal speed variation with a constant slope K_α . The lower limit is defined to prevent the control parameter α from reaching zero, as it would cause an indetermination in the control action.

4.2. Analysis of the MFC Adaptation

The analysis of the suitability of varying α with the vehicle's longitudinal speed can be carried out by analyzing the root locus of the feedback system (iPD controller—vehicle dynamics). To this end, a continuous-time expression of the MFC controller (4) and (5) and a linearized dynamic vehicle model are considered.

4.2.1. Continuous-Time MFC

Expressing the implicit temporal delay in (5) in continuous time yields the following transfer function of the iPD controller:

$$C_{iPD}(s) = \frac{U_{iPD}(s)}{E(s)} = \frac{K_p + K_d \cdot D(s) + D^2(s)}{\alpha \cdot (1 - e^{-T_s s})} \tag{8}$$

where $D(s) \triangleq \frac{s}{T_s s + 1}$ is a continuous-time-filtered derivative operator equivalent to (6) when $T = T_s C$.

The delay operator $e^{-T_s s}$ is substituted using its first-order Padé approximant to obtain the final expression of the MFC controller:

$$C_{iPD}(s) = \frac{K_p T^2 + K_d T + 1}{\alpha T_s} s^2 + \frac{2K_p T + K_d}{\alpha T_s} s + \frac{K_p}{\alpha T_s} \cdot \left(1 + \frac{T_s}{2} s\right) \tag{9}$$

4.2.2. Linearized Lateral Dynamic Vehicle Model

The vehicle’s lateral dynamics are linearly modeled as proposed in [27]:

$$\begin{bmatrix} \dot{y}_L \\ \dot{\psi}_L \\ \dot{\psi}_L \end{bmatrix} = \begin{bmatrix} 0 & 1 & 0 & 0 \\ 0 & -\frac{2C_f + 2C_r}{m v_x} & \frac{2C_f + 2C_r}{m} & -\frac{2C_f l_f + 2C_r l_r}{m v_x} \\ 0 & 0 & 0 & 1 \\ 0 & \frac{2C_r l_r - 2C_f l_f}{I_z v_x} & \frac{2C_f l_f - 2C_r l_r}{I_z} & -\frac{2C_f l_f^2 - 2C_r l_r^2}{I_z v_x} \end{bmatrix} \begin{bmatrix} y_L \\ \dot{y}_L \\ \psi_L \\ \dot{\psi}_L \end{bmatrix} + \begin{bmatrix} 0 \\ \frac{2C_f}{m} \\ 0 \\ \frac{2C_f l_f}{I_z} \end{bmatrix} \delta + \begin{bmatrix} 0 \\ -\frac{2C_f l_f - 2C_r l_r}{m v_x} - v_x \\ 0 \\ -\frac{2C_f l_f^2 + 2C_r l_r^2}{I_z v_x} \end{bmatrix} \dot{\psi}_{des} \tag{10}$$

where y_L and ψ_L are the lateral and angular deviations of the vehicle from the path, m is the vehicle mass, v_x is the longitudinal speed, C_r and C_f are the cornering stiffnesses of the rear and front wheels, l_r and l_f are the distances between the center of gravity (CoG) and the rear and front axle, I_z is the yaw inertia, δ is the steering angle, and $\dot{\psi}_{des}$ is the desired yaw rate. Table 1 presents the parameter values considered in this work, which are estimated from the experimental platform. Although real vehicles are substantially more complex, with strong nonlinearities and varying parameters, this model is commonly used in lateral control design (see [5,7] for an example).

Table 1. Vehicle’s dynamic parameters.

Parameter	m [kg]	I_z [kg·m ²]	C_f [N/rad]	C_r [N/rad]	l_f [m]	l_r [m]
Value	1372	1990	37,022.5	35,900	0.98	1.48

4.2.3. Root Locus of the Closed-Loop System

By using the controller in Equation (8) and the system dynamics described in (10), with the lateral deviation y_L as the output of the system and the dynamic parameters provided in Table 1, the closed-loop transfer function can be obtained. It should be noted that the term related to the desired yaw rate in (10) is considered a disturbance. Considering fixed values for the control parameters K_p and K_d , the root locus is obtained as a function of the longitudinal speed of the vehicle and the control parameter α , as shown in Figure 1. It should be noted that only the most significant poles are shown at the root locus.

As can be seen in Figure 1, the branches of the root locus cross the imaginary axis when α is low and the speed increases (see $\alpha = 300$ and $\alpha = 500$ in red and blue, respectively). This shows that the controlled system becomes unstable. It should be noted that the branches of the root locus end at 120 km/h. This condition is corrected when α is increased (see $\alpha = 1000$ and $\alpha = 1500$ in cyan and magenta, respectively), although the branches are closer to the imaginary axis for low and medium speeds, meaning that the controlled system is more oscillatory but remains stable for the considered speed range.

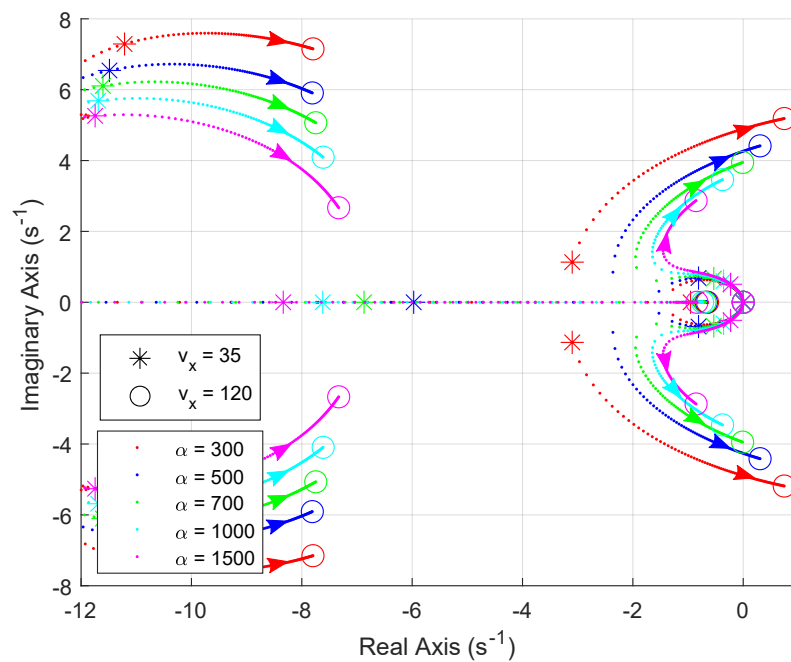


Figure 1. Root locus of the closed-loop system for various α when the longitudinal speed v_x is varied.

When the control parameter α is varied with the longitudinal speed according to (7), a new root locus can be plotted, as shown in Figure 2, where $K_\alpha = 20$, $v_{x,0} = 35$, and $\alpha_0 = 300$ are the parameters considered in (7). In this case, the most significant poles of the root locus (see $K_\alpha = 20$ in green in the Figure) are positioned closer to the real axis compared to when a low α is fixed, and they are located further toward the imaginary axis compared to when a high α is fixed. Consequently, the system remains stable and exhibits less oscillation within the considered speed range. It should be noted that the SAMFC formulation described in (7) is not linear but rather affine with lower saturation. This characteristic prevents the transformation of the controller into a unique transfer function, hence the root locus was obtained point-to-point.

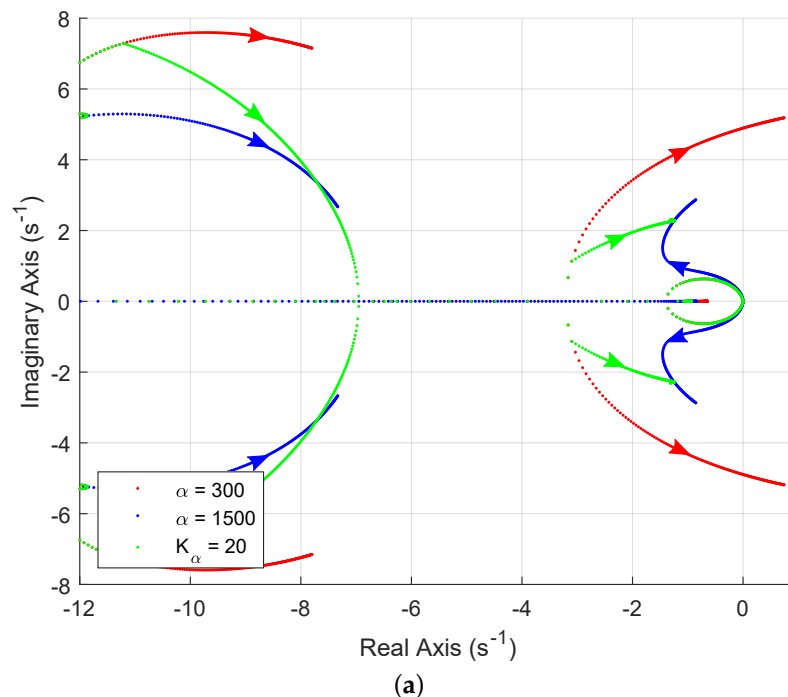


Figure 2. Cont.

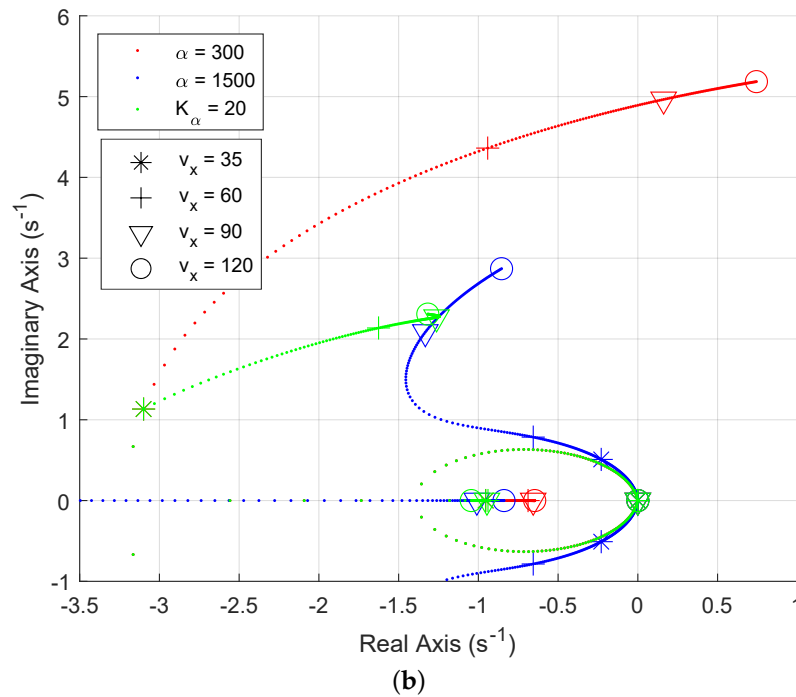


Figure 2. Root locus of the closed-loop system when α is a function of the longitudinal speed v_x . (a) Most significant poles of the root locus. (b) Detail of the root locus.

4.3. SAMFC Controller Design

In order to obtain the parameters of the SAMFC controller structure (7), a simple design procedure is proposed:

1. Obtain one standard MFC controller configuration ($\{K_p, K_d, \alpha_1\}$) for the maximum longitudinal speed of the application $v_{x,1}$.
2. Keeping K_p and K_d constant, reduce α until the closed-loop specifications are met for the minimum longitudinal speed of the application $v_{x,0}$, obtaining another MFC controller configuration ($\{K_p, K_d, \alpha_0\}$)
3. Obtain K_α from

$$K_\alpha = \frac{\alpha_1 - \alpha_0}{v_{x,1} - v_{x,0}} \tag{11}$$

4. Use α_0 and $v_{x,0}$ as the lower saturation parameters.

It should be noted that this design procedure relies on an MFC controller configuration for high speeds, which can be obtained using any available design procedure.

5. Results

In this section, a noniterative design procedure is applied (Section 5.4) using the simplified lateral dynamics model of the vehicle described in Section 4.2.2. The control configurations obtained are evaluated using the extended vehicle simulator described in Section 5.1, along with three metrics (defined in Section 5.3), across a wide range of driving contexts (described in Section 5.2). The performance of the resulting control configurations is compared in simulations to that of the parameter sets obtained with the iterative design procedure using the extended vehicle simulator (Section 5.7). To confirm the potential of the proposed control structure and design method, several experimental trials are conducted in an automated prototype, and the results are reported in Section 5.8.

5.1. Vehicle Extended Model

In order to ensure a faithful representation of the experimental platform outlined in [28], simulation tests were carried out using the same vehicle model described in [1]. The

dynamic model chosen for this purpose was a 14-degree-of-freedom system (6 for the vehicle body motion—longitudinal, lateral, vertical, roll, pitch, and yaw—and 8 for the wheels—vertical motion and spin of each wheel).

The powertrain model consisted of three components: (i) the engine, represented by its torque map, which was determined using the experimental platform data; (ii) the gearbox, which incorporates the same drive ratios and gear-shift logic as the actual vehicle; and (iii) the resistive torques from the braking system, wind forces acting longitudinally, and gravitational forces. The tire behavior was reproduced using the Pacejka tire model [29].

In addition to the electric power-assisted steering system already in place in the vehicle, an external actuation system was incorporated following the guidelines of [30]. To ensure the accuracy of the model, essential parameters such as inertia and backlash were measured or identified through extensive field tests. Moreover, the noise produced by the localization system of the experimental platform was characterized and included in the simulation model.

It should be noted that this model does not take into account climate conditions such as the wind effect or the state of the asphalt.

5.2. Benchmark Description

Figure 3 shows an aerial view of the two circuits used in the simulation and real-world tests. The trajectories T_1 and T_2 were designed to cover a wide range of realistic driving scenarios, including straight sections, curves of different natures, varying maximum speeds, and longitudinal and lateral accelerations. T_1 was designed as an urban scenario, including intersections and a roundabout, whereas T_2 was designed to emulate a regional road with higher-speed straight stretches and both slow and fast curves.

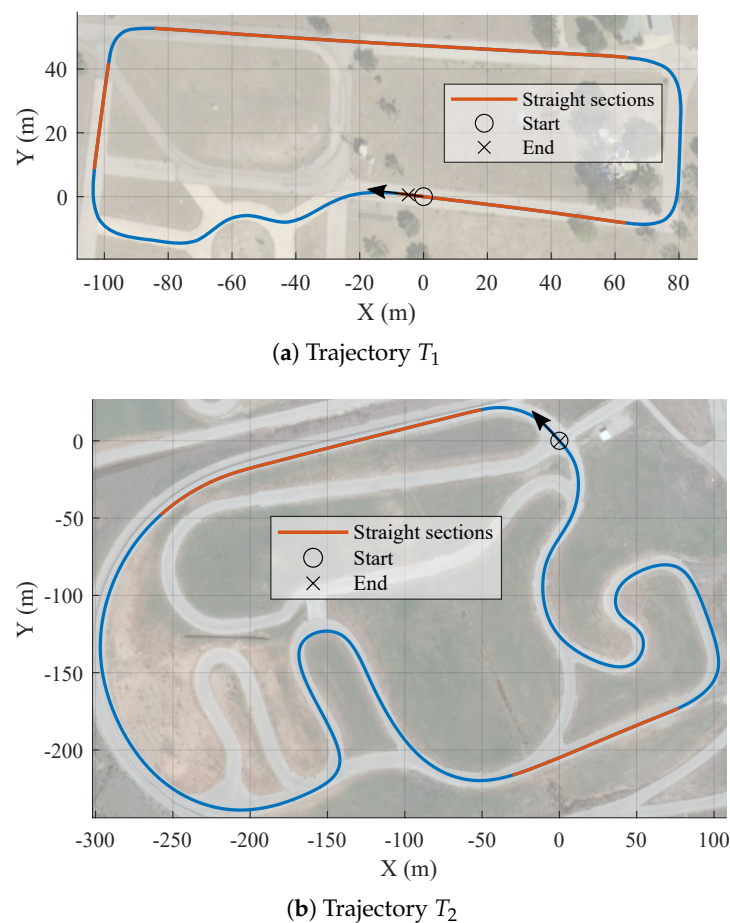


Figure 3. Benchmark trajectories.

To ensure the continuity of the curvature across the paths, they were defined by a cubic B-spline, which ensured C^2 continuity. Then, to generate the reference trajectories, speed profiles were computed for each path by applying the method for acceleration-limited speed planning proposed in [31]. The maximum speed and accelerations used to calculate the speed profile are shown in Table 2. The resulting speed profiles obtained are illustrated in Figure 4.

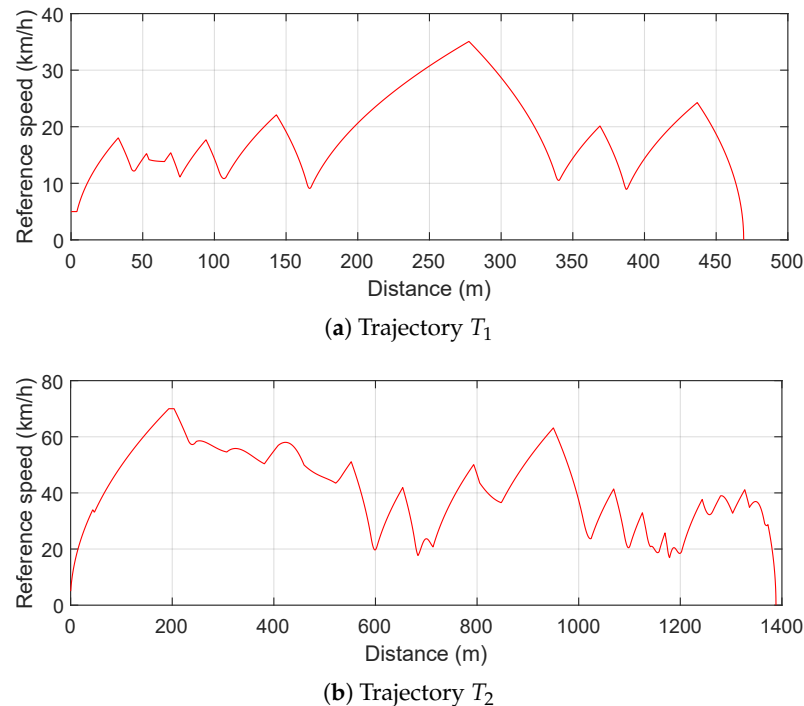


Figure 4. Speed profiles of the benchmark trajectories.

Table 2. Maximum speed and acceleration for each benchmark trajectory.

Trajectory	T_1	T_2
Maximum speed (km/h)	35	70
Maximum long. acceleration (m/s^2)	0.4	1.0
Maximum long. deceleration (m/s^2)	0.7	2.0
Maximum lat. acceleration (m/s^2)	1.0	2.0

5.3. Metrics Description

In this section, the metrics used to measure the performance of the controllers are analyzed in terms of tracking quality and control action. It should be noted that the metrics used in this work were introduced in [1].

The integral absolute lateral error (IAE) was used to assess tracking quality. However, to the best of the authors' knowledge, there has been no consensus on the metrics used to assess vehicle stability and passenger comfort (see Section 5.3 of [32] for a review of the different metrics used in the state-of-the-art literature). It was experimentally found that the classical IAU (Integral of the Absolute Value of the Control Action) and IAUD (Integral of the Absolute Value of the Derivative of the Control Action) were too simplistic to properly analyze the control action dynamics and they do not represent vehicle stability and passenger comfort. Therefore, an analysis of the frequency spectrum of the feedback control action was used to define two different performance indicators:

1. M_ϵ : this metric quantifies the low-frequency oscillations of the control action, which can lead to vehicle instability.

2. M_ζ : this variable quantifies the high-frequency oscillations of the control action, which can cause discomfort to the vehicle occupants.

The values of both metrics, M_ϵ and M_ζ , were computed in two separated frequency bands: ϵ (1.1–4 Hz) and ζ (4–10 Hz), respectively. It should be noted that a control frequency of 20 Hz was assumed in this work. A high-pass filter was initially applied to the feedback control action to remove unwanted spectral power values at low frequencies. The cutoff frequencies of these filters were 0.5 and 4 Hz for M_ϵ and M_ζ , respectively. Then, the spectrum was calculated by applying the short-time Fourier transform with 5-s overlapping sections.

The value of M_ϵ was finally calculated as the mean of the maximum power spectrum at each section, considering a scale factor and a threshold to balance the order of magnitude of both metrics:

$$M_\epsilon = \frac{1}{n} \sum_{i=1}^n s_\epsilon \cdot \max(10 \cdot \log P_{\epsilon,i} + \lambda_\epsilon) \quad (12)$$

where n is the amount of 5-s sections, $P_{\epsilon,i}$ is the spectrum power of band ϵ in section i , s_ϵ is a scale factor ($s_\epsilon = 0.015$), and λ_ϵ is a threshold in dB ($\lambda_\epsilon = 80$ dB).

The high sensitivity of M_ϵ can lead to incorrect metric values in curves due to its low-frequency spectrum. Therefore, only straight and long sections, where the path curvature is below 0.01 m^{-1} and the vehicle drives for more than 5 s (considering the speed profile of each trajectory), were considered. The straight sections for each test trajectory are highlighted in orange in Figure 3.

The procedure used to obtain M_ϵ was also applied to calculate M_ζ . However, instead of using the mean value, the maximum power among all sections was assigned to this metric, with a scale factor of $s_\zeta = 0.04$ and the same threshold of $\lambda_\zeta = 80$ dB. This particular choice was motivated by the low equivalence observed in the experimental tests between the intended interpretation of this metric and the value obtained when using the mean value. The experimental tests showed that when the mean value of all sections was used, the isolated occurrence of high frequencies caused the value of the metric to be low, even though the oscillations caused discomfort. When the maximum value within each section was used, the metric correctly indicated the presence of oscillations that caused discomfort. However, when the maximum power was considered, controllers that exhibited high-frequency oscillations in any section of the test trajectory had high values of M_ζ .

To summarize, IAE was the chosen indicator of reference tracking quality, M_ϵ was used to measure the (in)stability margin of the controller, and M_ζ was used to measure passenger discomfort.

To illustrate the magnitude of the performance metrics, it was experimentally observed that an IAE greater than 0.35 m implies poor path tracking in the curves, an M_ϵ greater than 0.25 implies the possibility of system instability when the speed is high, and an M_ζ greater than 0.7 indicates a loss of passenger comfort.

5.4. Standard MFC Parameter Design

The design procedure to obtain SAMFC configurations, which was introduced in Section 4.3, relies on control configurations of standard MFC controllers. Several approximations to the MFC controller design problem have been proposed [33–35]. In [33], an MFC tuning procedure using the least squares method was proposed. In [34], an α adaptation law for autonomous vehicle applications and a design method based on a quadratic cost index and a decision tree were proposed.

In this paper, the standard MFC controller configurations were obtained by applying the design procedure introduced in [35]. This method allows to obtain MFC controller configurations that meet user-defined time-response and frequency-response specifications. It is based on the relationship between MFC controllers and Three-Term Controllers, as well as the root-counting and phase-unwrapping formulas from [36].

It was proven in [35] that a three-term controller in its Z-transform representation

$$C_{PID}(z) = \frac{K_2z^2 + K_1z + K_0}{z(z - 1)} \tag{13}$$

and a second-order iPD controller in its Z-transform representation

$$C_{iPD}(z) = z \frac{K_p T_s^2 (Cz + 1 - C)^2 + K_d T_s (z - 1)(Cz + 1 - C) + (z - 1)^2}{\alpha T_s^2 (z - 1)(Cz + 1 - C)^2} \tag{14}$$

are related by

$$\begin{bmatrix} T_s^2 C^2 & T_s C & -T_s^2 K_2 \\ T_s^2 2C(1 - C) & T_s(1 - 2C) & -T_s^2 K_1 \\ T_s^2 (C - 1)^2 & T_s(C - 1) & -T_s^2 K_0 \end{bmatrix} \begin{bmatrix} K_p \\ K_d \\ \alpha \end{bmatrix} = \begin{bmatrix} -1 \\ 2 \\ -1 \end{bmatrix} \tag{15}$$

when the three-term controller (13) is applied to $G(z) \cdot \frac{z^2}{(Cz + 1 - C)^2}$, with $G(z)$ being the system to be controlled.

With this relationship, the design methods for three-term controllers collated in [36] can be applied. These procedures allow the designer to obtain the stabilizing set of the controller for a given system, i.e., the control parameter configurations that make the closed-loop stable. By using the stabilizing set for a three-term controller and (15), the stabilizing set for an MFC controller can be obtained. Finally, the design method described in Section 4.3 can be applied.

5.5. Feedforward Control

A feedforward term u_{ff} was added to the feedback control action u_{fb} to compensate the path curvature. This term was designed to lighten the load on the feedback controller when the vehicle enters a curved section. Then, the complete steering wheel control action can be expressed as

$$\delta_t = \delta_{max} \cdot (u_{ff} + u_{fb}) \tag{16}$$

The feedforward term was applied in [1,12] and depends on a kinematic model of the vehicle and the curvature of the path, as shown in Figure 5. In Figure 5, y_L is the lateral deviation at the preview point P_p , and d_p is the preview distance from the vehicle's CoG. It should be noted that the speed-based variable preview distance was considered to obtain the feedback control action such that $d_p = d_{p,0} + v_x \cdot t_p$, where $d_{p,0}$ is the minimum preview distance, t_p is the preview time, and $d_{p,0}$ and t_p are tunable parameters considered for the implemented controllers.

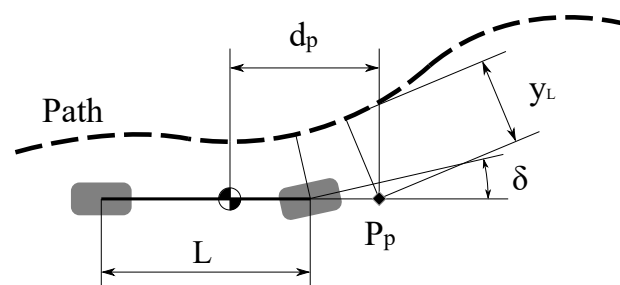


Figure 5. Kinematic model parameters.

Given these considerations, the feedforward controller is defined as

$$u_{ff} = \frac{R_S}{\delta_{max}} \cdot \arctan(L \cdot \kappa) \tag{17}$$

where the feedforward control action is normalized ($u_{ff} \in [-1, 1]$), L is the wheelbase, κ is the path curvature, R_s is the steering ratio, and δ_{max} is the maximum steering angle.

5.6. Control Configurations Evaluated

Two feedback control strategies were evaluated: the iPD (MFC) from Equations (4)–(6) and the Speed-Adaptive iPD (SAMFC) from Equations (4)–(7). Using these strategies, two evaluations were conducted: (i) to test the suitability of SAMFC, an iterative design procedure was applied to obtain the (SA)MFC controller configurations that optimized the performance metrics defined in Section 5.3, and (ii) to evaluate the results of the proposed design procedure (Section 5.4), it was applied to the vehicle model (10) to obtain different (SA)MFC controller configurations that were compared to those of the iterative procedure.

The tunable parameters of the evaluated strategies are

- MFC: K_p , K_d , α , $d_{p,0}$, and t_p
- SAMFC: K_p , K_d , α_0 , $v_{x,0}$, K_α , $d_{p,0}$, and t_p

5.6.1. Iteratively Designed Configurations

An iterative design procedure was applied to obtain an iPD controller configuration and an SAMFC controller configuration. These configurations minimized the performance metrics defined in Section 5.3 when evaluated on the benchmark trajectories (Section 5.2) using the extended vehicle simulator (Section 5.1). This design procedure was introduced in [1]. The control configurations obtained are shown in Table 3.

Table 3. MFC and SAMFC configurations obtained using the iterative design procedure.

Controller	K_p	K_d	α/α_0	K_α	v_0	$d_{p,0}$	t_p
iPD _{iter}	0	3.603	502.443	-	-	1.149	0
SAMFC _{iter}	0.75	2.766	93.603	10.0	12.783	0.625	0

5.6.2. Noniteratively Designed Configurations

It should be noted that, as the design method proposed in this work (Section 5.4) considers a dynamic vehicle model without a preview point, the values of $d_{p,0}$ and t_p are assumed to be zero ($d_{p,0} = t_p = 0$).

By applying the method described in Section 5.4 to the vehicle model (10), an iPD stabilizing set was obtained for high speeds (70 km/h). The stabilizing set obtained is shown in Figure 6. From this set, any configuration can be chosen by the designer. In this work, the configuration that could satisfy the most demanding frequency-response restrictions—namely, Gain Margin (GM) and Phase Margin (PM)—was chosen. It should be noted that the number of available configurations depends on the discretization step applied in the design procedure.

In order to obtain the configuration for low longitudinal speeds (20 km/h), the frequency response of the closed-loop system was evaluated at $v_x = 20$ km/h. The parameter α was adjusted by reducing its value (i.e., the controller was made more aggressive) until the margins at 20 km/h were similar to those of the high-speed configuration at 70 km/h, as described in Section 4.3. It should be noted that, although this part of the design procedure is iterative, only one parameter needs to be tuned, which can be done using information from the nominal model of the system.

Table 4 shows the selected configurations and their nominal frequency-response specifications. Using the procedure described in Section 4.3, an SAMFC controller was obtained from both low- and high-speed MFC configurations, as shown in Table 5.

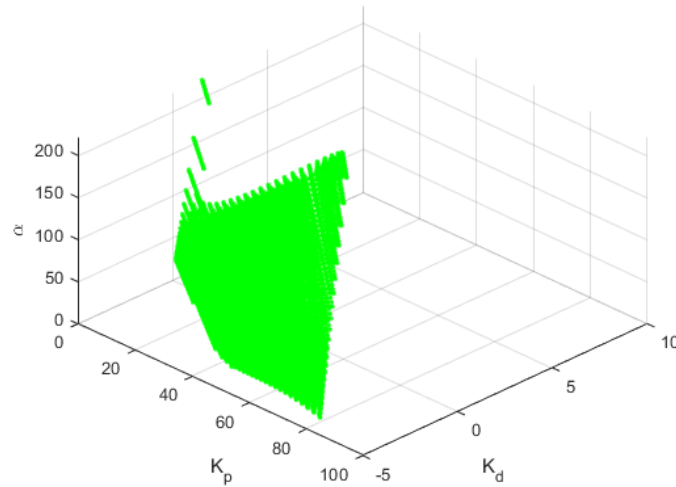


Figure 6. Stabilizing set for iPD controllers at longitudinal speed $v_x = 70$ km/h.

Table 4. iPD configurations obtained and their nominal frequency-response specifications.

Controller	K_p	K_d	α	GM	PM
iPD _H	0	0.8443	121.6	4.2	20.79
iPD _L	0	0.8443	40	2.16	59.27

Table 5. SAMFC control parameters.

Controller	K_p	K_d	α_0	K_α	$v_{x,0}$
SAMFC	0	0.8443	40	1.6320	20

The frequency-response specifications of the SAMFC controller designed for varying speeds are shown in Figure 7, where the dotted line in Figure 7b represents GM = 1. It can be observed that the SAMFC controller maintained greater consistency in both frequency-response specifications across the studied speed range than the MFC controllers used to design it. This characteristic indicates that the expected response will be uniform across different driving scenarios.

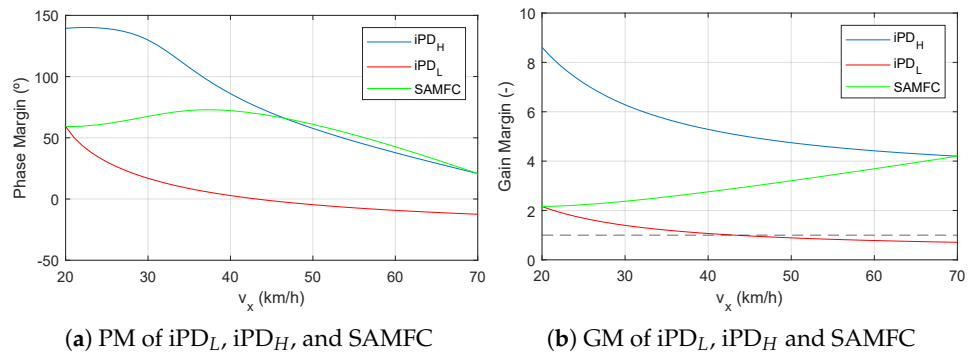


Figure 7. Frequency-response specifications as a function of longitudinal speed.

5.7. Simulation Results

In order to evaluate the performance of the five controllers obtained from both design procedures, simulations were conducted using the extended vehicle model (Section 5.1) on the two benchmark trajectories (Section 5.2). These trajectories cover a large number of

driving scenarios and have different driving dynamics. The performance of the controllers was evaluated using the performance metrics described in Section 5.3. The results are presented in Table 6.

Table 6. Extended vehicle model simulation results on the benchmark trajectories.

Controller	T_1			T_2		
	IAE	M_ϵ	M_ζ	IAE	M_ϵ	M_ζ
iPD _{iter}	0.207	0.067	0.167	0.054	0.112	0.203
SAMFC _{iter}	0.067	0.110	0.465	0.042	0.112	0.444
iPD _H	0.147	0.085	0.099	0.085	0.287	0.112
iPD _L	0.049	0.678	0.489	-	-	-
SAMFC	0.048	0.590	0.523	0.043	0.329	0.418

On the one hand, the iteratively designed SAMFC (SAMFC_{iter}) controller was able to improve the tracking quality metric (IAE) compared to the iteratively designed iPD (iPD_{iter}) controller while maintaining the stability and passenger comfort metrics (M_ϵ and M_ζ) within an acceptable range. On the other hand, the tracking quality of the noniteratively designed MFC controllers (iPD_H and iPD_L) was compromised when simulated on trajectories with different dynamic constraints from those for which they were originally designed. This effect was particularly pronounced in the case of iPD_L, where instability was observed in T_2 , as seen in Figure 7a,b. The noniteratively designed SAMFC controller exhibited better tracking quality than the MFC controllers from which it was originally obtained; however, there was a trade-off in passenger comfort (M_ζ).

The results in Table 6 show that (i) the SAMFC controller was able to improve the strategy of the standard MFC controller for the path-tracking control of an autonomous vehicle, and (ii) the proposed noniterative design procedure allowed to obtain competitive configurations with the information from a simplified vehicle model while being less computationally expensive than the iterative procedure.

5.8. Experimental Results

The vehicle used in the experiments was a Citroën DS3, which included hardware modifications for the automated control of the throttle, brake, gearbox, and steering systems (see Figure 8).



Figure 8. Experimental platform.

The localization of the vehicle relied on an RTK-DGPS receiver and onboard sensors to measure the vehicle's speed, accelerations, and yaw rate. An onboard computer with an Intel Core i7-8700T and 8Gb RAM was used to run the control algorithms. The vehicle was also equipped with exteroceptive sensors to perceive the environment [28].

To test the performance of the controllers in real environments, the controllers presented in Tables 3–5 were implemented on the experimental platform and tested on test tracks T_1 and T_2 . Although the tracking quality of the controllers in the real-world tests was slightly worse than in the simulations, the results (see Table 7) showed that the SAMFC controllers achieved better tracking quality than the MFC controllers. It should also be noted that the passenger comfort metric M_ζ was generally affected in the real-world tests due to differences between the vehicle extended model (Section 5.1) and the experimental platform.

Table 7. Real-world test results on the benchmark trajectories.

Controller	T_1			T_2		
	IAE	M_ϵ	M_ζ	IAE	M_ϵ	M_ζ
iPD _{iter}	0.23	0.02	0.13	0.12	0.10	0.37
SAMFC _{iter}	0.077	0.11	0.57	0.066	0.09	0.38
iPD _H	0.15	0.20	0.62	0.16	0.28	0.37
iPD _L	0.048	0.36	0.93	-	-	-
SAMFC	0.048	0.36	1.06	0.084	0.36	0.69

Figure 9 shows the performance of the iteratively designed MFC and SAMFC controllers and Figure 10 shows the behavior of the noniteratively designed SAMFC controller, as well as the MFC controllers from which it was originally designed, on the benchmark trajectory T_1 . As can be seen, the SAMFC controllers exhibited a lower Maximum Lateral Error (MLE) than the respective standard MFC controllers.

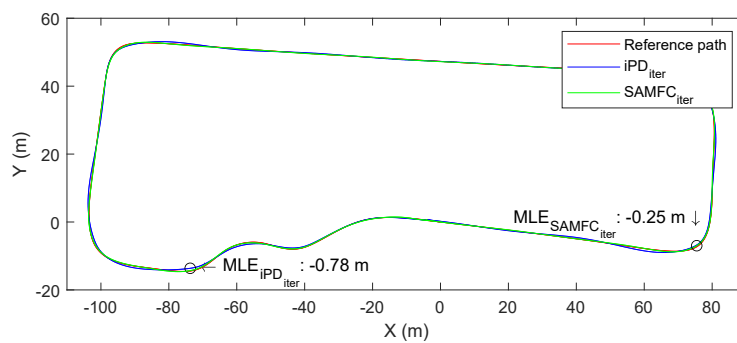


Figure 9. Iteratively designed (SA)MFC tracking results on trajectory T_1 .

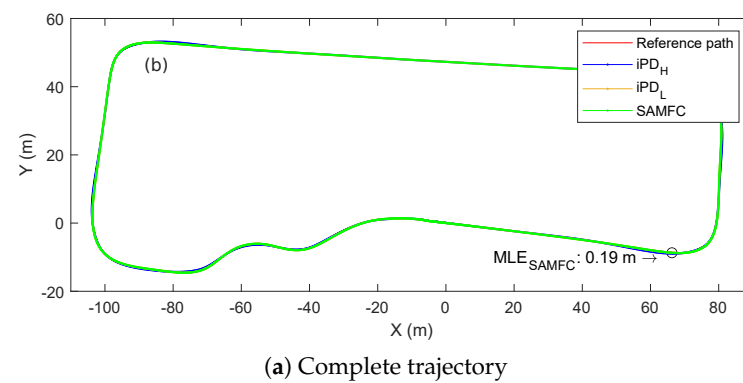
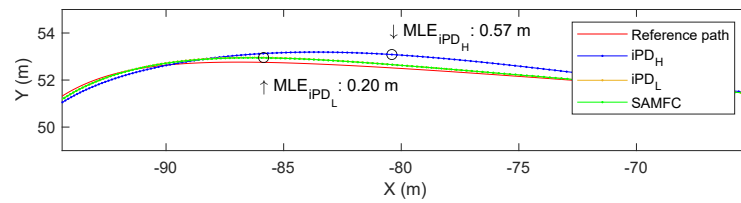


Figure 10. Cont.



(b) Detail of the path at (b)

Figure 10. Noniteratively designed (SA)MFC tracking results on trajectory T_1 .

Figure 11 shows the lateral errors of the five evaluated controllers on the benchmark trajectory T_1 . As can be observed, iPD_L and SAMFC exhibited similar tracking quality, performing better than the other tested controllers.

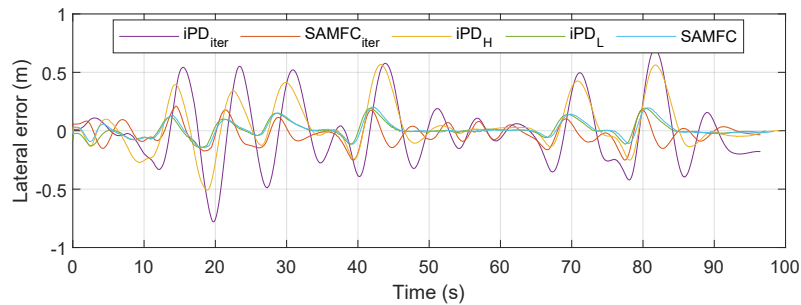


Figure 11. Lateral error over time on trajectory T_1 .

Figure 12 shows the control actions generated by the five controller configurations tested on benchmark trajectory T_1 . It can be seen that controllers with a low α (iPD_L and SAMFC) exhibited chattering due to the backlash of the steering actuator. This chattering in the control action did not affect the stability of the feedback system at the longitudinal speeds reached on this trajectory.

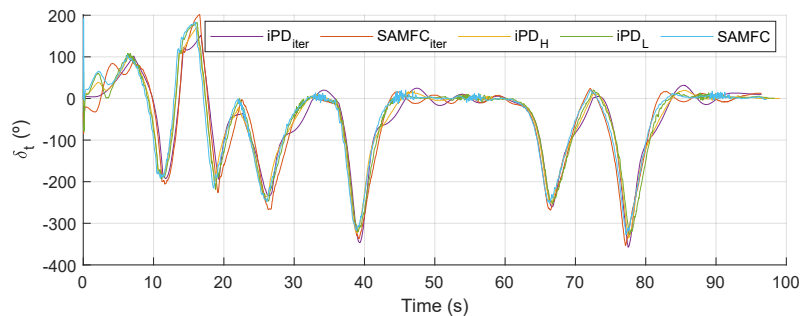


Figure 12. Controllers' actions on trajectory T_1 .

Figure 13 shows the performance of the iteratively designed MFC and SAMFC controllers and Figure 14 shows the performance of the noniteratively designed MFC and SAMFC controllers tested on benchmark trajectory T_2 . As can be seen, both SAMFC controllers exhibited lower Maximum Lateral Error (MLE) values than the respective original MFC controllers.

Figure 15 shows the lateral errors of the four evaluated controllers on benchmark trajectory T_2 . It should be noted that iPD_L became unstable in the simulation when tested on this trajectory so it was not tested on the experimental platform. As can be seen, the lateral error obtained using the noniteratively designed SAMFC controller was lower than that of the other controllers, which is shown in Table 7.

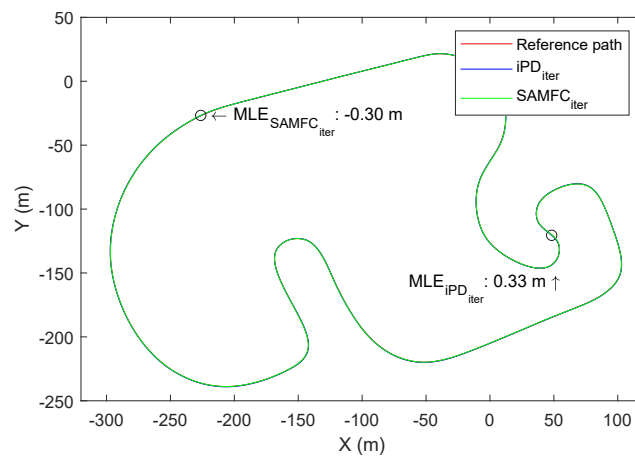


Figure 13. Iteratively designed (SA)MFC tracking results on trajectory T_2 .

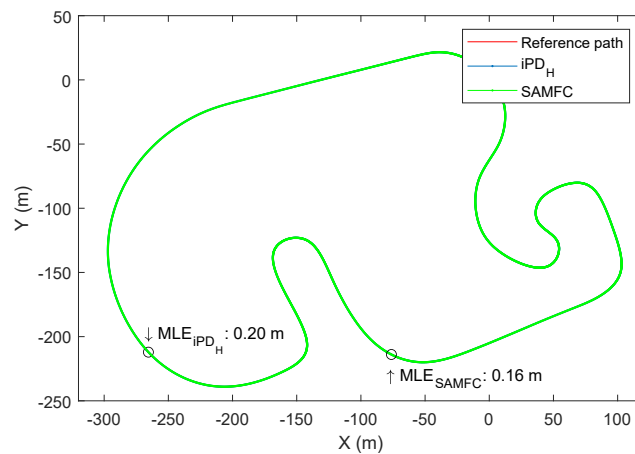


Figure 14. Noniteratively designed (SA)MFC tracking results on trajectory T_2 .

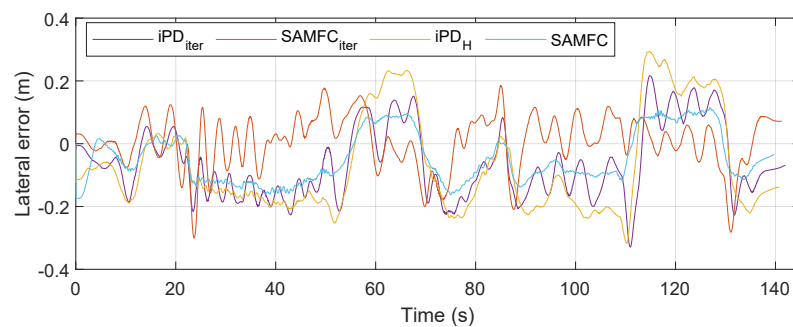


Figure 15. Lateral error over time on trajectory T_2 .

Figure 16 shows the control actions generated by the four controller configurations tested on benchmark trajectory T_2 . It can be seen that all the controllers generated some chattering due to the backlash of the steering actuator. However, it did not affect the stability of the feedback system, as observed on T_1 and reflected in the M_ϵ values. On the other hand, controllers with a variable α generated a more aggressive response at low speeds than those with a fixed α but they tended to correct the lateral error faster.

Trajectory T_2 had a very different shape, dynamic constraints, and speed profile from T_1 , which was quantitatively reflected in the metrics and the responses of the standard MFC controllers, as shown in Table 7. On the contrary, the Speed-Adaptive MFC controllers exhibited a more consistent response on both trajectories.

The results presented in this section were obtained on dry asphalt on a sunny day using healthy tires. It should be noted that changing these conditions may affect the reproducibility of the results.

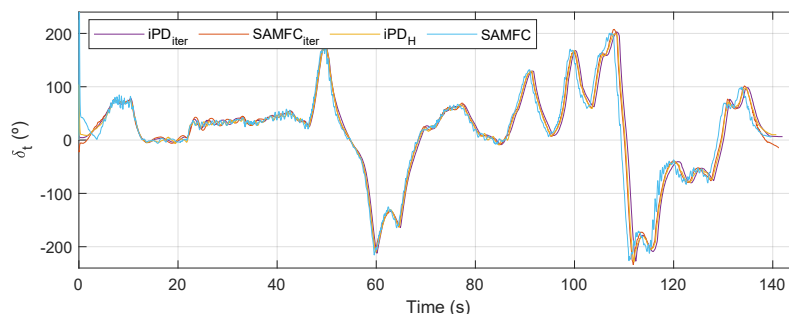


Figure 16. Controllers' actions on trajectory T_2 .

6. Conclusions

The results obtained in simulation and real-world tests, together with the theoretical analysis of the suitability of the variation of the MFC control parameter, prove that Speed-Adaptive Model-Free Control is capable of improving the tracking quality compared to standard Model-Free Control while maintaining its performance characteristics across a wider range of longitudinal speeds. The proposed design method has been tested and it has been proven to be easily applied. The SAMFC configuration obtained through this method exhibits a more aggressive behavior that can improve the tracking quality of autonomous vehicles while ensuring acceptable levels of passenger comfort.

Author Contributions: Conceptualization, J.V., C.J. and M.F.; methodology, J.V.; software, M.M.-G. and A.A.; validation, A.A. and M.M.-G.; formal analysis, M.M.-G., C.J. and M.F.; investigation, M.M.-G. and A.A.; resources, J.V. and M.F.; writing—original draft preparation, M.M.-G.; writing—review and editing, J.V.; visualization, A.A. and M.M.-G.; supervision, C.J. and M.F.; project administration, J.V.; funding acquisition, J.V. All authors have read and agreed to the published version of the manuscript.

Funding: This research was partially supported by the joint CNRS (France)-CSIC (Spain) PICS Program through the project UbiMFC (CoopIntEer 203 073).

Institutional Review Board Statement: Not applicable.

Data Availability Statement: Data sharing not applicable.

Acknowledgments: The authors would like to thank the Instituto Nacional de Técnica Aeroespacial (INTA) for providing the opportunity to use their test tracks to conduct some of the experiments presented in this work.

Conflicts of Interest: The authors declare no conflict of interest.

Abbreviations

The following abbreviations are used in this manuscript:

GM	Gain Margin
IAE	Integral Absolute (Lateral) Error
IAU	Integral of the Absolute Value of the Control Action
IAUD	Integral of the Absolute Value of the Derivative of the Control Action
MFC	Model-Free Control(ler)
MLE	Maximum Lateral Error
MPC	Model Predictive Control
PID	Proportional–Integral–Derivative (Controller)
PM	Phase Margin
SAMFC	Speed-Adaptive Model-Free Control(ler)
ULMPC	Ultra-Local Model Predictive Control

References

1. Moreno-Gonzalez, M.; Artuñedo, A.; Villagra, J.; Join, C.; Fliess, M. Speed-adaptive model-free lateral control for automated cars. In Proceedings of the Joint IFAC Conference: SSSC-TDS-LPVS, Montreal, QC, Canada, 27–30 September 2022; IFAC: New York, NY, USA, 2022.
2. Fliess, M.; Join, C. Model-free control. *Int. J. Control* **2013**, *86*, 2228–2252. [[CrossRef](#)]
3. Villagra, J. Chapter 8—Interplay between decision and control. In *Decision-Making Techniques for Autonomous Vehicles*; Villagra, J., Jiménez, F., Eds.; Elsevier: Amsterdam, The Netherlands, 2023; pp. 193–213.
4. Arifin, B.; Suprpto, B.Y.; Prasetyowati, S.A.D.; Nawawi, Z. The Lateral Control of Autonomous Vehicles: A Review. In Proceedings of the International Conference on Electrical Engineering and Computer Science, Batam, Indonesia, 2–3 October 2019; pp. 277–282.
5. Zainal, Z.; Rahiman, W.; Baharom, M. Yaw rate and sideslip control using pid controller for double lane changing. *J. Telecommun. Electron. Comput. Eng.* **2017**, *9*, 99103.
6. Liu, Q.; Liu, Y.; Liu, C.; Chen, B.; Li, L.; Ji, X. Hierarchical Lateral Control Scheme for Autonomous Vehicle with Uneven Time Delays Induced by Vision Sensors. *Sensors* **2018**, *18*, 2544. [[CrossRef](#)] [[PubMed](#)]
7. Jiang, J.; Astolfi, A. Lateral Control of an Autonomous Vehicle. *IEEE Trans. Intell. Veh.* **2018**, *3*, 228–237. [[CrossRef](#)]
8. Kapsalis, D.; Sename, O.; Milanés, V.; Martínez, J.J. Gain-scheduled steering control for autonomous vehicles. *IET Control Theory Appl.* **2020**, *14*, 3451–3460. [[CrossRef](#)]
9. Zanon, M.; Frasch, J.V.; Vukov, M.; Sager, S.; Diehl, M. Model Predictive Control of Autonomous Vehicles. In *Optimization and Optimal Control in Automotive Systems*; Springer: Cham, Switzerland, 2014; pp. 41–57.
10. Laghmar, H.; Boudali, M.T.; Laurain, T.; Ledy, J.; Orjuela, R.; Lauffenburger, J.P.; Basset, M. Obstacle Avoidance, Path Planning and Control for Autonomous Vehicles. In Proceedings of the IEEE Intelligent Vehicles Symposium, Paris, France, 9–12 June 2019; pp. 529–534.
11. Marcano, M.; Díaz, S.; Matute, J.A.; Irigoyen, E.; Pérez, J. A cascade steering shared controller with dual-level dynamic authority. *IFAC-PapersOnLine* **2020**, *53*, 15353–15359. [[CrossRef](#)]
12. Godoy, J.; Pérez, J.; Onieva, E.; Villagrà, J.; Milanés, V.; Haber, R. A driverless vehicle demonstration on motorways and in urban environments. *Transport* **2015**, *30*, 253–263. [[CrossRef](#)]
13. Wang, X.; Fu, M.; Ma, H.; Yang, Y. Lateral control of autonomous vehicles based on fuzzy logic. *Control Eng. Pract.* **2015**, *34*, 1–17. [[CrossRef](#)]
14. Jin, X.; Yin, G.; Wang, J. Robust fuzzy control for vehicle lateral dynamic stability via Takagi-Sugeno fuzzy approach. In Proceedings of the American Control Conference, Seattle, WA, USA, 24–26 May 2017; pp. 5574–5579.
15. Park, M.W.; Lee, S.W.; Han, W.Y. Development of lateral control system for autonomous vehicle based on adaptive pure pursuit algorithm. In Proceedings of the 2014 14th International Conference on Control, Automation and Systems (ICCAS 2014), Seoul, Republic of Korea, 22–25 October 2014; pp. 1443–1447.
16. Villagra, J.; d’Andréa Novel, B.; Choi, S.; Fliess, M.; Mounier, H. Robust stop-and-go control strategy: An algebraic approach for non-linear estimation and control. *Int. J. Veh. Auton. Syst.* **2009**, *7*, 270–291. [[CrossRef](#)]
17. Villagra, J.; Herrero-Perez, D. A Comparison of Control Techniques for Robust Docking Maneuvers of an AGV. *IEEE Trans. Control Syst. Technol.* **2012**, *20*, 1116–1123. [[CrossRef](#)]
18. Ziane, M.A.; Pera, M.; Join, C.; Benne, M.; Chabriat, J.; Steiner, N.Y.; Damour, C. On-line implementation of model free controller for oxygen stoichiometry and pressure difference control of polymer electrolyte fuel cell. *Int. J. Hydrogen Energy* **2022**, *47*, 38311–38326. [[CrossRef](#)]
19. Guilloteau, Q.; Robu, B.; Join, C.; Fliess, M.; Rutten, É.; Richard, O. Model-free control for resource harvesting in computing grids. In Proceedings of the CCTA 2022, Trieste, Italy, 23–25 August 2022.
20. Menhour, L.; d’Andréa Novel, B.; Fliess, M.; Mounier, H. Multivariable decoupled longitudinal and lateral vehicle control: A model-free design. In Proceedings of the IEEE Conference on Decision and Control, Firenze, Italy, 10–13 December 2013; pp. 2834–2839.
21. Fliess, M.; Lévine, J.; Martin, P.; Rouchon, P. Flatness and defect of non-linear systems: Introductory theory and examples. *Int. J. Control* **1995**, *61*, 1327–1361. [[CrossRef](#)]
22. Wang, Z.; Wang, J. Ultra-local model predictive control: A model-free approach and its application on automated vehicle trajectory tracking. *Control Eng. Pract.* **2020**, *101*, 104482. [[CrossRef](#)]
23. Wang, Z.; Zhou, X.; Wang, J. Extremum-seeking-based adaptive model-free control and its application to automated vehicle path tracking. *IEEE/ASME Trans. Mechatron.* **2022**, *27*, 3874–3884. [[CrossRef](#)]
24. Carrillo, F.J.; Rotella, F. Some contributions to estimation for model-free control. *IFAC-PapersOnLine* **2015**, *48*, 150–155. [[CrossRef](#)]
25. Safaei, A.; Mahyuddin, M.N. Adaptive model-free control based on an ultra-local model with model-free parameter estimations for a generic SISO system. *IEEE Access* **2018**, *6*, 4266–4275. [[CrossRef](#)]
26. Wang, H.; Xu, H.; Tian, Y.; Tang, H. α -Variable adaptive model free control of iReHave upper-limb exoskeleton. *Adv. Eng. Softw.* **2020**, *148*, 102872. [[CrossRef](#)]
27. Rajamani, R. *Vehicle Dynamics and Control*; Springer Science & Business Media: Berlin/Heidelberg, Germany, 2011.

28. Artuñedo, A.; Godoy, J.; Villagra, J. A decision-making architecture for automated driving without detailed prior maps. In Proceedings of the 2019 IEEE Intelligent Vehicles Symposium (IV), Paris, France, 9–12 June 2019; IEEE: Piscataway, NJ, USA; pp. 1645–1652.
29. Pacejka, H.; Bakker, E. The magic formula tyre model. *Veh. Syst. Dyn.* **1992**, *21*, 1–18. [[CrossRef](#)]
30. Lee, D.; Kim, K.S.; Kim, S. Controller Design of an Electric Power Steering System. *IEEE Trans. Control Syst. Technol.* **2018**, *26*, 748–755. [[CrossRef](#)]
31. Artuñedo, A.; Villagra, J.; Godoy, J. Jerk-Limited Time-Optimal Speed Planning for Arbitrary Paths. *IEEE Trans. Intell. Transp. Syst.* **2021**, *23*, 8194–8208. [[CrossRef](#)]
32. Stano, P.; Montanaro, U.; Tavernini, D.; Tufo, M.; Fiengo, G.; Novella, L.; Sorniotti, A. Model predictive path tracking control for automated road vehicles: A review. *Annu. Rev. Control* **2022**, *55*, 194–236. [[CrossRef](#)]
33. Yahagi, S.; Kajiwara, I. Non-Iterative Data-Driven Tuning of Model-Free Control Based on an Ultra-Local Model. *IEEE Access* **2022**, *10*, 72773–72784. [[CrossRef](#)]
34. Hegedűs, T.; Fényes, D.; Németh, B.; Szabó, Z.; Gáspár, P. Design of Model Free Control with tuning method on ultra-local model for lateral vehicle control purposes. In Proceedings of the 2022 American Control Conference, Atlanta, GA, USA, 8–10 June 2022; IEEE: Piscataway, NJ, USA; pp. 4101–4106.
35. Moreno-Gonzalez, M.; Villagra, J. Model-Free Control Design Procedure Applied to Lateral Vehicle Control. In Proceedings of the 22nd IFAC World Congress 2023, Yokohama, Japan, 9–14 July 2023.
36. Bhattacharyya, S.P.; Datta, A.; Keel, L.H. *Linear Control Theory: Structure, Robustness, and Optimization*; CRC Press: Boca Raton, FL, USA, 2018.

Disclaimer/Publisher’s Note: The statements, opinions and data contained in all publications are solely those of the individual author(s) and contributor(s) and not of MDPI and/or the editor(s). MDPI and/or the editor(s) disclaim responsibility for any injury to people or property resulting from any ideas, methods, instructions or products referred to in the content.